

Chapter 7

Coupling-current induced field distortions

This chapter deals in particular with the additional magnetic fields caused by the interstrand coupling currents (ISCCs) and the boundary-induced coupling currents (BICCs) during a field sweep of coils made of multistrand conductors. Field distortions caused by the interfilament coupling currents and a non-uniform current distribution are briefly discussed.

Field \mathbf{B}_{is} caused by the ISCCs is calculated starting from the ISCC-distribution as determined in chapter 6. The spatial distribution of the cross-contact resistance R_c in the coils determines which harmonic components are influenced. A minimum R_c -value can be defined in order to ensure that the field induced by the ISCCs remains below the acceptance limit determined by the magnet specifications.

The field \mathbf{B}_{bi} caused by the BICCs is shown to vary sinusoidally along the magnet axis. The magnitude of the distortions is strongly influenced by small variations in the magnet length, transposition pitch, R_c -distribution and effective strand resistivity and is therefore very difficult to calculate.

Methods are discussed by which the fields \mathbf{B}_{is} and \mathbf{B}_{bi} can be distinguished from the fields caused by the filament magnetisation, the fabrication tolerances and a non-uniform current distribution.

Experimental results are presented of \mathbf{B}_{is} and \mathbf{B}_{bi} in 1 m and 10 m long LHC dipole model magnets. The magnitudes of the harmonic components of \mathbf{B}_{is} are evaluated and compared with calculated values based on the average R_c in the coils. The magnitude and the characteristic time of \mathbf{B}_{bi} will be dealt with, and an estimate is made of the characteristic length of the BICCs and the effective strand resistivity.

7.1 Introduction

Especially in accelerator magnets, field distortions are of a major concern since the particle motion becomes unstable above certain values of the higher harmonics, resulting in considerable beam losses and a smaller luminosity. Correction magnets are present in accelerators and are especially suitable for correcting the field distortions that are the same for all magnets.

A good understanding of the field distortions requires a classification of the various fields that contribute to the total field in the aperture of a magnet and the origins from which these fields are created. In superconducting coils made of monolithic conductors the field distortions are dominated by the following three components:

- The field \mathbf{B}_{geo} related to fabrication tolerances of the various components. This field changes during excitation of the magnet, since the electromagnetic forces change and cause a deformation of the coils.
- The field \mathbf{B}_m caused by the persistent currents in the filaments is, in first approximation, proportional to the filament diameter and the critical current density $J_c(B, T)$. The field quality of superconducting magnets at low excitation is therefore strongly influenced by the persistent currents since the critical current density is large. This phenomenon is well understood and experimental results and calculations are usually in good agreement (see for example [Caspi, '87], [Wanderer, '93], [Zhao, '93]) provided that the $J_c(B, T)$ relation is sufficiently known. If the properties of the superconductor are uniform, field \mathbf{B}_m follows the symmetry of the main field so that only the normal odd harmonics B_1, B_3, \dots are present. The time dependence of the persistent currents, which is related to flux creep in the superconductor [Anderson, '62], [Kim, '62], is, however, less defined. Experimental results on the time dependence of the persistent currents in the Tevatron [Finley, '87] and in HERA [Brück, '90] have shown a logarithmic decay in time with a characteristic change of a few percent per decade. Measurements on short cable pieces show a similar decay although the time dependence is less pronounced, see e.g. [Gilbert, '89], [Marken, '92].
- The field \mathbf{B}_{if} , produced by the IFCCs, is linear with the central-field-sweep rate and inversely proportional to the effective transverse resistivity of the strand and decreases at higher levels of excitation due to the magnetoresistance of the matrix.

While the preceding field distortions are well understood, the use of multistrand cables in accelerator magnets has caused additional field errors that exhibit an anomalous time dependence during and after field sweeps. Sinusoidal variations in the axial direction of the magnet have been observed in HERA magnets, where the amplitude and phase depend strongly on the actual and preceding excitation cycles of the magnet [Brück, '91a/'91b]. Results on a RHIC prototype dipole magnet show that the axial variations are caused by unbalanced currents and not by magnetisation of the filaments [Sampson, '95]. Measurements on SSC dipole magnets at BNL have shown that the amplitude of the axial variations depends on the central-field-sweep rate \dot{B}_{ce} if the contact resistance R_c is small, while the amplitude is almost independent of \dot{B}_{ce} if R_c is large [Ghosh, '93/'94]. Measurements on the SSC magnets have also shown that the amplitude of the periodic

pattern during the ramp increases with time [Devred, '94]. Since the first observation at HERA, the sinusoidally varying field errors are thought to be related to a *Non-Uniform Current Distribution (NUCD)* among the strands due to different joint resistances, locally very small R_c and differences between the inductances of the strands. However, the observed effects could not be explained by the existing models. With the new description of the BICCs as presented in chapter 5, it is possible to describe the additional field distortions in cabled superconductors by three types of fields:

- The field \mathbf{B}_{is} caused by the ISCCs, which is proportional to the central-field-sweep rate \dot{B}_{ce} and, in first approximation, inversely proportional to the average contact resistance R_c between the strands. This linear dependence of \mathbf{B}_{is} on \dot{B}_{ce} and $1/R_c$ has been observed in SSC dipole magnets [Ogitsu, '92a/'92b/'93/'94]. In section 7.4 it will be shown that especially the higher harmonics depend strongly on the spatial R_c -distribution in the coils. The measured multipole components of \mathbf{B}_{is} of several SSC dipole magnets are used to estimate the R_c -distribution over the cross-section of the coils in these magnets [Devred, '94].
- The field \mathbf{B}_{nucd} caused by a non-uniform distribution of the transport current among the strands, mainly due to differences between the joint resistances of the strands (see section 5.2). Field \mathbf{B}_{nucd} is invariant to \dot{B}_{ce} and can depend on the excitation level due to the magnetoresistance of the connections. Field \mathbf{B}_{nucd} has a periodic pattern along the magnet length with a period equal to the cable pitch.
- The field \mathbf{B}_{bi} , caused by the BICCs, is proportional to \dot{B}_{ce} . Also \mathbf{B}_{bi} varies sinusoidally along the magnet axis with a period equal to the cable pitch. Field \mathbf{B}_{bi} can be large if large gradients in the field-sweep rate are present along the cable in the coil.

The total field in the aperture of a magnet can be regarded as a superposition of the various field components:

$$\mathbf{B} = \mathbf{B}_{tr} + \mathbf{B}_{geo} + \mathbf{B}_m + \mathbf{B}_{if} + \mathbf{B}_{nucd} + \mathbf{B}_{is} + \mathbf{B}_{bi} \quad [\text{T}], \quad (7.1)$$

with \mathbf{B}_{tr} the field produced by the transport current, flowing uniformly in the cable. The coupling-current induced field error \mathbf{B}_{cc} is given by those components that are proportional to \dot{B}_{ce} :

$$\mathbf{B}_{cc} = \mathbf{B}_{if} + \mathbf{B}_{is} + \mathbf{B}_{bi} \quad [\text{T}]. \quad (7.2)$$

This chapter mainly deals with these three field distortions quantified in the straight part of the magnet.

In section 7.2 the methods are presented by which the fields \mathbf{B}_{if} , \mathbf{B}_{is} and \mathbf{B}_{bi} are calculated. In sections 7.3-7.5 the magnitudes of \mathbf{B}_{if} , \mathbf{B}_{is} and \mathbf{B}_{bi} are presented for the particular case of LHC dipole magnets. It is shown that when R_c of the cable is specified, predictable and limited, the lower field harmonics of \mathbf{B}_{is} can meet the requirements concerning the field quality of a magnet. The effect of a non-uniform R_c between the two poles of an aperture on field \mathbf{B}_{is} is dealt with. Large variations in R_c between the two poles of an aperture are deduced from the loss measurements as presented in chapter 6. It is shown that the magnitude of \mathbf{B}_{bi} is hard to assess since the BICCs are caused by numerous \dot{B} - and R_c -variations in the various turns of the coils.

In section 7.6 several methods are discussed by which the coupling-current induced fields can be determined and distinguished from each other. Experimental results are presented of the field errors \mathbf{B}_{cc} observed in four LHC dipole magnets. An estimate is given of the individual components \mathbf{B}_{is} and \mathbf{B}_{bi} by analysis of the time dependence and variations in the axial direction of field \mathbf{B}_{cc} .

7.2 Calculating coupling-current induced field distortions

Field \mathbf{B}_{if}

According to eqs. 3.18 and 3.20, the IFCCs in a strand with a round cross-section, subject to a ramped field $\dot{B}_{\perp s}$ normal to the strand axis (i.e. in the y -direction), can be represented by two net coupling currents:

$$I_{if} = \pm \frac{2\tau_{if} d_s^*}{\mu_0} \dot{B}_{\perp s} \quad [\text{A}], \quad (7.3)$$

flowing at either side of the strand. In order to calculate the field caused by these currents, they are located at their centre of gravity, i.e. at distances $x = \pm \pi d_s^*/8$ from the centre of the strand [Avest, ter, '91]. The currents I_{if} in the strands of a coil turn will gradually increase and decrease since the field varies across the cable width. It is therefore more convenient to calculate the field \mathbf{B}_{if} taking the currents in each *strand position* (see Fig. 5.5) instead of the currents in each *strand*. The small field contribution in the z -direction is disregarded here because the fields in the z -direction caused by all the strand currents in the cable cancel almost completely (at least in the straight part of the magnet).

According to the law of Biot and Savart, the field at a position $\mathbf{z} = x + iy$ caused by a current I_{if} at position $\mathbf{r} = x_1 + iy_1$ is:

$$\mathbf{B}_{if} = \frac{\mu_0 I_{if}}{2\pi(\mathbf{z} - \mathbf{r})} \quad [\text{T}]. \quad (7.4)$$

The iron yoke which surrounds the collars enhances the field. When the yoke is not saturated, its permeability is uniform, and the inner boundary is a perfect cylinder. The increase in the field can then be calculated using the image-current method [Hague, '62], which implies that for a line current I located at position \mathbf{r} inside a yoke of radius R_{ir} and relative permeability μ , an image current I^* with magnitude:

$$I^* = \frac{\mu - 1}{\mu + 1} I \cong I \quad [\text{A}] \quad \text{for } \mu \gg 1, \quad (7.5)$$

is located at position:

$$\mathbf{r}^* = \frac{R_{ir}^2}{r^2} \mathbf{r} \quad [\text{m}]. \quad (7.6)$$

The field \mathbf{B}_{if} caused by the current I_{if} is thus the sum of the fields created by the current itself and the image current:

$$\mathbf{B}_{if} = \frac{\mu_0}{2\pi} \left(\frac{I_{if}}{(\mathbf{z} - \mathbf{r})} + \frac{I_{if}^*}{(\mathbf{z} - \mathbf{r}^*)} \right) \quad [\text{T}]. \quad (7.7)$$

In the aperture of a magnet, where $|\mathbf{z}| < |\mathbf{r}|$, eq. 7.7 can be expanded into a Taylor series:

$$\mathbf{B}_{if} = -\frac{\mu_0 I_{if}}{2\pi} \left(\frac{1}{\mathbf{r}} \sum_{n=1}^{\infty} (\mathbf{z}/\mathbf{r})^{n-1} + \frac{1}{\mathbf{r}^*} \sum_{n=1}^{\infty} (\mathbf{z}/\mathbf{r}^*)^{n-1} \right) \quad [\text{T}]. \quad (7.8)$$

Eq. 7.8 can be rewritten as:

$$\begin{aligned} \mathbf{B}_{if} &= -\frac{\mu_0 I_{if}}{2\pi \mathbf{r}} \sum_{n=1}^{\infty} \left(1 + (r/R_{ir})^{2n} \right) (\mathbf{z}/\mathbf{r})^{n-1} \\ &= -\frac{\mu_0 I_{if}}{2\pi r_0} \sum_{n=1}^{\infty} \left(1 + (r/R_{ir})^{2n} \right) (r_0/\mathbf{r})^n (\mathbf{z}/r_0)^{n-1} \quad [\text{T}], \end{aligned} \quad (7.9)$$

showing that all multipoles are present in the field produced by a single line current. The total field \mathbf{B}_{if} in a magnet is calculated by summation of the individual fields (i.e. eq. 7.9) over all the strand positions in each turn of the cross-section of the coils.

Field \mathbf{B}_{is}

In chapter 4 it is shown that the ISCCs can be regarded as currents flowing along a zigzag path parallel to the cable axis. Away from the cable, the field produced by the zigzag currents can be well approximated by an infinitely long straight current-line I_s located at the centre of the zigzag path and normal to the x - y plane. Again, the small contribution of the field in the z -direction is disregarded.

The field \mathbf{B}_{is} caused by the zigzag current I_s is then calculated in exactly the same way as the field \mathbf{B}_{if} in the case of a current I_{if} . The total field is calculated by summation of all the fields caused by all the ISCCs in each turn of the coil.

Field \mathbf{B}_{bi}

The field errors caused by the BICCs are difficult to calculate. First of all, the BICCs in the whole magnet have to be calculated taking into account the R_c - and \hat{B}_\perp -distributions along the cable length and across the cable width. Each strand is then subdivided into four segments per cable pitch corresponding to the four faces of the cable (see Fig. 7.1).

In a strand segment the BICC is assumed to be constant which is valid if $\xi \gg L_{p,s}/2$ (regime A, see eq. 5.4) or $l_{cab} \gg L_{p,s}/2$ (regime B, see eq. 5.9). The field at the origin caused by a current I_{bi} in a segment situated between the positions $\mathbf{r}_1 = (x_1, y_1, z_1)$ and $\mathbf{r}_2 = (x_2, y_2, z_2)$ satisfies [Durand, '68]:

$$\mathbf{B}_{bi} = \frac{\mu_0 I_{bi}}{4\pi} \frac{(r_1 + r_2) \mathbf{r}_1 \times \mathbf{r}_2}{r_1 r_2 (r_1 r_2 + \mathbf{r}_1 \cdot \mathbf{r}_2)} \quad [\text{T}]. \quad (7.10)$$

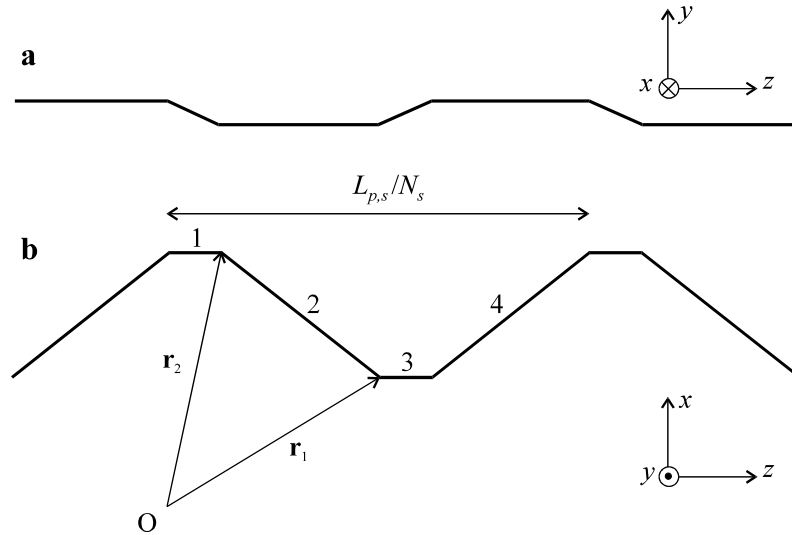


Figure 7.1. Calculation of the field in point O caused by a current in a strand of a Rutherford-type cable by considering the four faces of the cable separately. **a.** front view of the side face. **b.** front view of the top face.

The total field in the aperture of the magnet is calculated by summation of the fields produced by the BICCs of each strand segment of each turn. The z -component of \mathbf{B}_{bi} is disregarded since the fields in the z -direction caused by the four strand segments cancel almost completely.

A multipole expansion of \mathbf{B}_{bi} of the order n is obtained by a Fourier analysis of the fields calculated on at least $2n$ places at a given radius relative to the magnet axis. All multipole components of \mathbf{B}_{bi} exhibit a characteristic time which is related to the characteristic time $\tau_{bi,av}$ of the BICCs. An upper limit of the time constant can be estimated using Fig. 5.16 or eq. 5.14, assuming that the BICCs flow through the entire cable. For example the maximum τ_{bi} for the inner coil of a 1 m long LHC dipole model with $N_s=26$, $L_{p,s}=0.13$ m, $R_c=4 \mu\Omega$, $l_{cab,1}=l_{cab,2}=12$ m is of the order of 10^4 s. The characteristic time can be considerably smaller if the BICCs decay quasi-exponentially and can be estimated using eq. 5.13. The characteristic time can also be reduced due to the mutual interaction between the BICCs of neighbouring turns as discussed in section 5.4.3.

Field \mathbf{B}_{nucd}

The field caused by a NUCD among the strands is calculated in exactly the same way as the field \mathbf{B}_{bi} . The magnitudes of all the multipole components are unpredictable, since the joint resistances are unknown and the fields caused by the BICCs in the various turns partially cancel. Field \mathbf{B}_{nucd} is proportional to the transport current if the ratio between the joint resistances of the strands is independent of the excitation level, up to currents near the critical current, where the strand resistivity itself starts to affect the total strand resistance (see section 5.2).

7.3 Field \mathbf{B}_{if} in dipole magnets

The field \mathbf{B}_{if} of two LHC dipole magnet designs is calculated for a central-field-sweep rate $\dot{B}_{ce}=0.01 \text{ Ts}^{-1}$. The matrix resistivity is assumed to be constant over the cross-section of the coil so that τ_{if} is also constant. This implies that, during a field sweep, besides a current I_{if} at position (r, ϕ) , a current I_{if} is also present at $(r, -\phi)$ and currents of magnitude $-I_{if}$ at $(r, \pi-\phi)$ and at $(r, \pi+\phi)$. Therefore, the I_{if} -distribution follows the symmetry of the main field so that only the normal odd harmonics B_1, B_3, B_5, \dots are generated.

The multipole components of \mathbf{B}_{if} are presented in Table 7.1 at the reference position $x_0=0.01 \text{ m}$, $y_0=0$ in the aperture of the magnet and for a characteristic τ_{if} of 0.025 s (see Table 3.2).

Similar to the IFCCs, field \mathbf{B}_{if} is proportional to \dot{B}_{ce} and τ_{if} . As a comparison, the total field \mathbf{B}_m due to the persistent currents in the filaments of the strands is also given at a central field of 0.58 T and a temperature of 1.9 K (calculations of the separate contributions for each block are given in [Wolf, '92]).

The results clearly show that for the PBD and WBD magnets, all the multipole components of \mathbf{B}_{if} are more than one order of magnitude smaller than those of \mathbf{B}_m . During operation of LHC, the relative harmonic components of \mathbf{B}_{if} at the start of the ramp (with $B_{inj}=0.58 \text{ T}$, $\dot{B}_{ce}=0.0066 \text{ Ts}^{-1}$) are smaller than 10^{-5} while at higher excitation levels they further decrease by more than one order of magnitude. Therefore, the influence of the IFCCs on the field homogeneity of high-field accelerator magnets is negligible.

Table 7.1. Absolute field errors \mathbf{B}_{if} and \mathbf{B}_{is} for two LHC dipole designs at $x_0=0.01 \text{ m}$, $y_0=0$ for $\tau_{if}=0.025 \text{ s}$, $R_c=1 \mu\Omega$, $L_{p,s}=0.1 \text{ m}$ and $\dot{B}_{ce}=0.01 \text{ Ts}^{-1}$. As a comparison, the field \mathbf{B}_m (at 1.9 K) due to the persistent currents is included for $B_{ce}=0.58 \text{ T}$, calculated for the given filament diameters [Verweij, '92/'94]. Note that the units vary from 10^{-4} T to 10^{-6} T .

Pink Book Dipole magnet.		Inner coil: $d_f=5 \mu\text{m}$.			Outer coil: $d_f=5 \mu\text{m}$.			\mathbf{B}_m Total
n	Units	\mathbf{B}_{if} Inner coil	Outer coil	Total	\mathbf{B}_{is} (see section 7.4) Inner coil Outer coil		Total	
B_1	10^{-4} T	+0.10	+0.041	+0.14	+58	+7.3	+65	-4.2
B_3	10^{-4} T	-0.044	-0.013	-0.057	+2.0	+0.1	+2.1	-2.3
B_5	10^{-5} T	+0.065	-0.0068	+0.058	-1.8	-0.31	-2.1	+1.5
B_7	10^{-6} T	-0.031	+0.0031	-0.028	-0.018	+0.0036	-0.015	-0.92
B_9	10^{-6} T	+0.015	+0.00017	+0.015	+0.43	+0.007	+0.44	+0.41
White Book Dipole magnet.		Inner coil: $d_f=7 \mu\text{m}$.			Outer coil: $d_f=6 \mu\text{m}$			\mathbf{B}_m Total
n	Units	\mathbf{B}_{if} Inner coil	Outer coil	Total	\mathbf{B}_{is} (see section 7.4) Inner coil Outer coil		Total	
B_1	10^{-4} T	+0.052	-0.011	+0.041	+51	+9.1	+60	-6.3
B_3	10^{-4} T	-0.024	-0.013	-0.037	+1.6	+0.016	+1.6	-2.1
B_5	10^{-5} T	+0.033	-0.0019	+0.031	-0.34	-0.24	-0.57	+1.0
B_7	10^{-6} T	-0.046	+0.0035	-0.043	-0.82	+0.15	-0.67	-1.8
B_9	10^{-6} T	+0.012	-0.000015	+0.012	+0.24	+0.0026	+0.25	+0.43

7.4 Field B_{is} in dipole magnets

It is shown in section 4.4.1 that the ISCCs in a Rutherford-type cable are mainly caused by a field change \dot{B}_\perp normal to the cable width. The steady-state distribution of the ISCCs across the cable width for a uniform \dot{B}_\perp is given by eq. 4.20:

$$I_s(x) = 0.0415 \frac{L_{p,s} w N_s}{R_c} \dot{B}_\perp \cos(\pi x / w) \quad [\text{A}], \quad (7.11)$$

where x varies between w/N_s and $(w-w/N_s)$. The sinusoidal pattern of the ISCCs is slightly influenced if \dot{B}_\perp varies across the cable width and is strongly influenced if \dot{B}_\perp changes sign across the width (see section 4.7). The steady-state ISCCs can be calculated for each turn taking into account the local \dot{B}_\perp -distribution across the cable width. The field change $\dot{B}_{\perp,i}$ for turn i can then be written as a function of the central-field-sweep rate \dot{B}_{ce} :

$$\dot{B}_{\perp,i} = \beta_{I,i} \dot{B}_{ce} \quad [\text{Ts}^{-1}], \quad (7.12)$$

with $\beta_{I,i}$ the field geometry factor that depends on the shape of the field variation \dot{B}_\perp across the cable width of turn i . The $\beta_{I,i}$ -values are shown in Fig. 7.2.

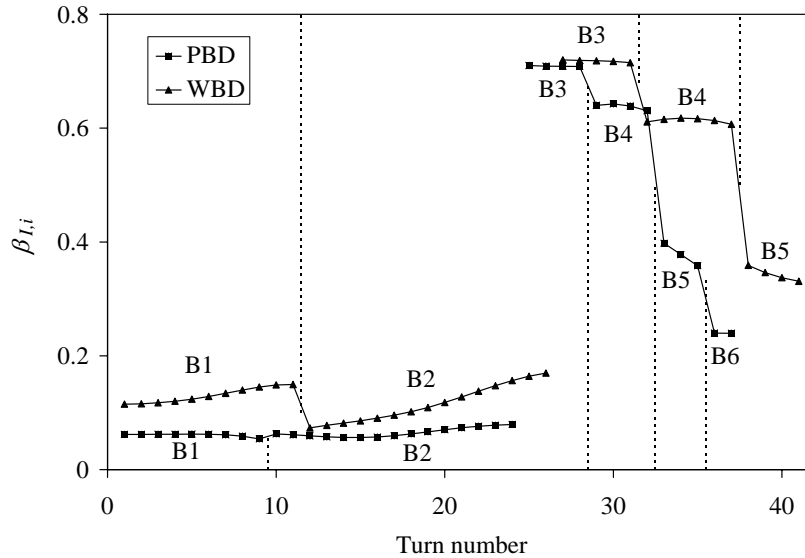


Figure 7.2. The field geometry factor β_I for each turn of the PBD and WBD magnets. The labels indicate the block number.

The maximum β_I of about 0.7 occurs near the midplane and is a representative value of accelerator dipole magnets with a ‘two-shell’ geometry (see section 2.2). The β_I -values of blocks 1 and 2 can be used to calculate the maximum ISCC in each turn but the pattern is no longer sinusoidal because \dot{B}_\perp changes sign across the cable width. The distribution of the ISCCs over the cross-section of one quadrant of the 5-block LHC dipole design (WBD

magnet) is illustrated in Fig. 7.3. In the case of excitation of the magnet, the ISCCs near the aperture for the inner coil, and almost everywhere in the outer coil have the same sign as the transport current. During de-excitation the ISCCs reverse sign while the transport current, of course, does not.

Figure 7.3. The distribution of the ISCCs over the cross-section of a WBD magnet with constant R_c in the coils. The dark colours indicate large positive or negative currents.

The I_s -distribution in a dipole coil with a symmetric R_c -distribution around the midplane also follows the symmetry of the main field, similar to the IFCCs, so that only the normal odd harmonics B_1, B_3, B_5, \dots are generated. These multipoles are calculated for the PBD and WBD magnets with $R_c=1 \mu\Omega$ and $L_{p,s}=0.1$ m and presented in Table 7.1. Similar to the ISCCs, the field errors are proportional to $L_{p,s}$ and \dot{B}_{ce} and inversely proportional to R_c . The difference between the fields \mathbf{B}_{is} of the two designs is small. Field \mathbf{B}_{is} is much larger than field \mathbf{B}_{if} (for $R_c < 10 \mu\Omega$), especially for the lower harmonics. Hence, field \mathbf{B}_{if} can be neglected in eq. 7.2 compared to field \mathbf{B}_{is} for all the dipole model magnets given in Table 2.3.

The relative dipole component at small excitation levels is large which causes a difference between the dynamic and static main-field component at the start of the ramp. This causes a tune shift since the fundamentals of the quadrupole and dipole magnets may change considerably at the start of the ramp. In the case of the LHC dipole magnets R_c

should be at least 50-100 $\mu\Omega$ to achieve an acceptable tune shift at the start of the ramp, assuming a constant field-sweep rate $\dot{B}_{ce}=0.0066 \text{ Ts}^{-1}$ [Verweij, '94]. Also the relative sextupole component of \mathbf{B}_{is} is a few times 10^{-4} at the start of the ramp and is of the same order but opposite to that of field \mathbf{B}_m . An R_c -value larger than 10 $\mu\Omega$ is preferable in order to keep all the higher multipole components of \mathbf{B}_{is} about one order of magnitude smaller than those of \mathbf{B}_m . The results, as surveyed in Table 7.1, show that the main contribution to field \mathbf{B}_{is} is related to the ISCCs in the inner coil. Hence, especially the R_c of the inner coil has to be sufficiently large in order to meet the field specifications of a 'two-shell' magnet.

A decrease of the field-sweep rate (especially near injection, where the relative field errors are large) also reduces \mathbf{B}_{is} since the ISCCs are proportional to \dot{B}_{ce} . This, however, decreases the effective running time of the accelerator and very small field-sweep rates should therefore be avoided.

Not only should the mean R_c in a coil be limited but differences in R_c between the magnets in the accelerator also have to be restricted in order to limit the variation in the main field between magnets (especially at the start of the ramp). A good reproducibility of R_c in all the cables of the magnets is necessary to meet this requirement.

The calculated dipole and sextupole components of \mathbf{B}_{is} of other accelerator dipole magnets (with a 'two-shell' geometry) are presented in Table 7.2.

Table 7.2. The absolute multipole components B_1 and B_3 caused by the ISCCs calculated for several accelerator dipole magnets at $x_0=0.01 \text{ m}$, $y_0=0$. The central field increases at a rate of 0.01 Ts^{-1} . The fields are calculated for a uniform R_c of $1 \mu\Omega$ as well as a uniform R_c^* of $2.6 \mu\Omega\text{mm}^2$ (see eq. 4.27).

	LHC (PBD)	LHC (WBD)	SSC ^a	HERA	Tevatron ^a	RHIC ^a
Central field (T)	10	8.4	6.6	4.7	4.4	3.5
Cable width (mm)	17	15	12	10	7.8	9.7
Nr. of strands	26	28	30	24	23	30
$L_{p,s}$ (mm)	100	100	86	95	66	73
$R_c = 1 \mu\Omega$						
B_1 (10^{-4} T)	65	60	62	17 (16 ^a)	6	7
B_3 (10^{-4} T)	2.1	1.6	4	0.8 (0.7 ^a)	0.3	0.4
$R_c^* = 2.6 \mu\Omega\text{mm}^2$						
B_1 (10^{-4} T)	65	45	28	11	2	2
B_3 (10^{-4} T)	2.1	1.2	1.8	0.5	0.1	0.1

^a [Devred, '94]

The field errors of the various magnets cannot be simply scaled to the cable geometry since field \mathbf{B}_{is} is a complicated function of both the cable geometry and the magnet geometry such as the number of turns and the diameter of the aperture. Note that R_c of the magnets will probably be rather different, even for identical surface conditions of the strand, since the average contact area of R_c varies significantly (see eq. 4.33). The fields are therefore also calculated for constant R_c^* , following $R_c = R_c^* (N_s^2 - N_s) / (L_{p,s} w)$ (see eq. 4.27). The latter values give a better picture of the variations in the field errors between the magnets for strands

with the same surface conditions. It is clear that the dipole and sextupole components increase strongly for an increase in the cable width. In practical accelerator dipole magnets (with a ‘two-shell’ geometry) the cable width is, in first approximation, proportional to the central field (see Fig. 1.1). An important conclusion is therefore that the contact resistance of a cable has to be larger to meet the field specifications in accelerator dipole magnets with a larger field. For ‘three- or four-shell’ geometries R_c can be relatively smaller.

Additional field distortions caused by the ISCCs are present if R_c varies over the cross-section of the coils. In the case that both poles of an aperture have different contact resistances $R_{c,p1}$ and $R_{c,p2}$, skew-even multipoles are induced (as illustrated in section 2.2), which are given in Table 7.3 for the PBD and WBD magnets.

Table 7.3. Absolute field errors \mathbf{B}_{is} for LHC dipole magnets at $x_0=0.01$ m, $y_0=0$ for $\dot{B}_{ce}=0.01$ Ts⁻¹, $R_{c,p1}=2/3 \mu\Omega$, $R_{c,p2}=2 \mu\Omega$ and $L_{ps}=0.1$ m. The normal-odd multipoles are exactly the same as those given in Table 7.1. Note that the units vary from 10⁻⁴ T to 10⁻⁶ T.

	Units	PBD			WBD		
		Inner coil	Outer coil	Total	Inner coil	Outer coil	Total
A_2	10 ⁻⁴ T	-17	-1.6	-18	-15	-2.4	-17
A_4	10 ⁻⁴ T	-1.9	-0.094	-2.0	-1.4	-0.11	-1.5
A_6	10 ⁻⁵ T	-1.4	+0.0075	-1.4	-1.1	+0.00026	-1.1
A_8	10 ⁻⁶ T	-1.3	+0.0046	-1.3	-0.56	-0.023	-0.59

While the normal-odd harmonics are proportional to $(1/R_{c,p1}+1/R_{c,p2})$, the skew-even harmonics are proportional to $(1/R_{c,p1}-1/R_{c,p2})$. This implies that the sign of the normal-odd harmonics is likely to be equal for all the magnets in an accelerator while the sign of the skew-even multipoles of \mathbf{B}_{is} will vary from magnet to magnet if differences in R_c of the two poles have a non-systematic cause. Table 7.3 shows that especially the A_2 and A_4 components of \mathbf{B}_{is} are large compared to values of a few times 10⁻⁴ which are usually regarded as just acceptable. Hence, the difference between the average R_c of the two poles of an aperture has to be limited in order to meet the field specifications of the magnets. These harmonics can be reduced by one order of magnitude by using either cables with $R_c > 10 \mu\Omega$ or cables for which R_c is almost constant and uniform so that $|1/R_{c,p1}-1/R_{c,p2}| < 10^5 \Omega^{-1}$.

In practical coils each turn of each quadrant of an aperture is likely to have a different average R_c , which implies that a field sweep will also result in normal-even and skew-odd multipoles. In theory, the R_c -distribution over the cross-section of the magnet can then be calculated if the multipole components of \mathbf{B}_{is} are known. In practice, even for small R_c , \mathbf{B}_{is} can only be determined up to about ten multipoles which implies that there are much more unknown local R_c -values than known multipole components. Only with additional assumptions (such as minimisation of the difference in R_c between adjacent turns) can a rough estimate of the R_c -distribution be obtained. The measured multipole components of \mathbf{B}_{is} in several SSC dipole magnets have been used to estimate the R_c -distribution over the cross-section of the coils in the magnet [Ogitsu, '92a], [Devred, '94]. This approach is not

used in this chapter since the results would be too speculative, especially if field \mathbf{B}_{bi} is large compared to \mathbf{B}_{is} .

7.5 Field \mathbf{B}_{bi} in dipole magnets

It can be calculated (using the method as described in section 7.2) that the field \mathbf{B}_{bi} caused by the BICCs in a single straight cable varies with a sinusoidal shape along the cable. Field \mathbf{B}_{bi} in a magnet is caused by many BICCs flowing in each turn, and will also have a sinusoidal shape since a superposition of sine functions is also a sine function.

The magnitude of the BICCs (and therefore the amplitude of \mathbf{B}_{bi}) is, however, difficult to calculate since it depends strongly on the R_c - and ρ_s -distributions over the cross-section of the coils, which are both more or less unknown. Furthermore, according to section 5.5, the magnitude of the BICCs depends strongly on the ratio between the length of the field variations with respect to the cable pitch. Consider, for example, the BICCs caused by the two coil ends in one turn of a 10 m long dipole magnet, with a straight part of $100L_{p,s}$. The magnitude of the BICCs could change completely if the number of twist pitches in the straight part of the magnet between the two coil ends changes by 0.5. An increase (decrease) of only 0.5% in $L_{p,s}$, which implies that the straight part would correspond to $99.5L_{p,s}$ ($100.5L_{p,s}$), results in a considerable change in the magnitude of the BICCs, and hence \mathbf{B}_{bi} (unless, of course, the BICCs decay with a characteristic length smaller than about half the magnet length, i.e. $\xi < 50L_{p,s}$ in this case). Since the fabrication tolerances of the cable pitch are often larger than 0.5%, the field \mathbf{B}_{bi} in similar magnets can be rather different.

The following remarks can be made:

- The amplitude of the multipole components of \mathbf{B}_{bi} in high-field accelerator dipole magnets can easily attain values of 10^{-4} to 10^{-3} T for $\dot{B}_{ce} = 0.01 \text{ Ts}^{-1}$. Simulations show that large BICCs usually result in large values of *all* multipoles of \mathbf{B}_{bi} . It is, however, possible that only some harmonics are affected while others are not.
- The phase of the sinusoidally varying field \mathbf{B}_{bi} is usually different for each harmonic component.
- An amplitude modulation in \mathbf{B}_{bi} will occur if the transposition twists of the cables in the inner and outer coils are different since, in that case, the period of the BICC pattern in both coils is different.
- Large skew-even multipoles of \mathbf{B}_{bi} are likely to occur due to the 180° symmetry in the aperture (i.e. the two splices are located at 180° from each other, so either in quadrants Q1 and Q3 or in quadrants Q2 and Q4, see Fig. 2.2a). This implies that, if a BICC is present at position (r, ϕ) it is likely that a BICC is also present at position $(r, \pi + \phi)$, which corresponds to the characteristic current pattern of skew-even multipoles.

Note that, although the amplitude of field \mathbf{B}_{bi} can be large, the integral value of \mathbf{B}_{bi} over the entire length of the magnet is almost zero. The effect of sinusoidally varying fields on the particle motion is not well-known and it is beyond the scope of this thesis to investigate this. In section 7.7.5 the field \mathbf{B}_{bi} , as estimated from the field distortion \mathbf{B}_{cc} , in four LHC dipole model magnets is presented in order to have a first quantitative estimate of the magnitude of the field.

7.6 Experimental methods to determine \mathbf{B}_{cc}

In the aperture of a magnet, only the sum of the magnetic fields caused by all the currents in the coil can be measured as given by eq. 7.1. Common methods to measure this field are:

- Rotating pick-up coils (RPCs). The voltage over a coil, rotating in the aperture, is integrated over given angular intervals. The main field harmonics can be determined using a fast Fourier transformation of the integrated voltages. Detailed descriptions of the method are given in the literature (for example [Walckiers, '92]).
- Fixed pick-up coils (FPCs). Integration of the voltage over a non-rotating coil gives the flux perpendicular to the coil surface. A field of order n can be determined by a combination of n FPCs located at intermediate angles of $360^\circ/n$ in accordance with Fig. 2.1.
- Hall probes. A specific multipole component can be determined with n Hall probes in a similar configuration to that for the FPCs.

The various contributions to the total field (see eq. 7.1) can be separated by considering the characteristics of the currents that cause them. In Table 7.4 these characteristics with respect to the excitation level, the field-sweep rate and the z -position are presented. The characteristic time denotes the period during which the fields decay once the field sweep is finished.

Table 7.4. Survey of the characteristics of the various field distortions in superconducting magnets. The characteristic times are typical values calculated in the case of an LHC dipole magnet.

Field	Origin	Dependence on the field	Dependence on \dot{B}_{ce}	Dependence on the z -position	Char. time
\mathbf{B}_{geo}	Fabr. tolerances	Yes	No	Possible, but not sinusoidal	$\rightarrow 0$
\mathbf{B}_m	Pers. currents	Yes	No	No	$\rightarrow \infty^a$
\mathbf{B}_{if}	IFCCs	Yes	Linear	No	< 0.2 s
\mathbf{B}_{nucd}	NUCD	Yes	No	Sinusoidal with period $L_{p,s}$	$\gg 10$ s
\mathbf{B}_{is}	ISCCs	No	Linear	Possible, but not sinusoidal	< 10 s
\mathbf{B}_{bi}	BICCs	Yes	Linear	Sinusoidal with period $L_{p,s}$	$\gg 10$ s

^a The estimated effect of the flux creep is about 2% per decade in time

According to Table 7.4, the fields \mathbf{B}_{geo} , \mathbf{B}_m , \mathbf{B}_{if} and \mathbf{B}_{is} , that do not vary sinusoidally in the axial direction can be determined with a RPC or FPC with a coil length equal to $k \cdot L_{p,s}$ ($k=1, 2, 3, \dots$). A combination of two Hall probes spaced $(k+0.5)L_{p,s}$ apart in the axial direction is also insensitive to the magnitudes of \mathbf{B}_{nucd} and \mathbf{B}_{bi} (if the amplitudes of \mathbf{B}_{nucd} and \mathbf{B}_{bi} are z -independent). For small field-sweep rates, the measured field errors are dominated by \mathbf{B}_{geo} and \mathbf{B}_m which can be separated since:

- \mathbf{B}_m is relatively large at weak excitation levels while \mathbf{B}_{geo} is relatively large at strong excitation levels.
- The persistent currents at 1.8 K are significantly larger than those at 4.3 K (at the same field) since the critical current at 1.9 K is about 50% larger than at 4.3 K. Field \mathbf{B}_{geo} remains unchanged between 4.3 K and 1.9 K.

The ramp-rate-dependent fields \mathbf{B}_{if} and \mathbf{B}_{is} can be determined by measuring the field as a function of the field-sweep rate, as illustrated in Fig. 7.4. Fields \mathbf{B}_{if} and \mathbf{B}_{is} cannot be separated experimentally. The R_c -values of the magnets of which the field errors are presented in section 7.7 are smaller than $10 \mu\Omega$ so that \mathbf{B}_{if} is negligible compared to \mathbf{B}_{is} (see Table 7.1).

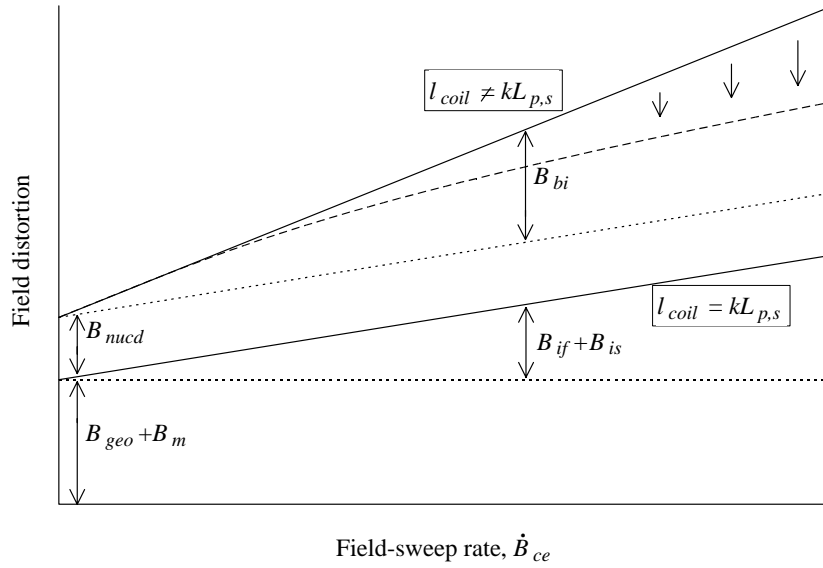


Figure 7.4. The various field distortions as functions of the field-sweep rate for different lengths of the pick-up coil. The arrows \downarrow indicate that field \mathbf{B}_{bi} becomes smaller than the steady-state value if the time of the field sweep is small compared to the characteristic time of the BICCs.

Fields \mathbf{B}_{nucd} and \mathbf{B}_{bi} can be deduced from a field measurement with a coil length unequal to $kL_{p,s}$. Both fields can be separated by performing field measurements as a function of the field-sweep rate as illustrated in Fig. 7.4. The most accurate method to deduce \mathbf{B}_{nucd} and \mathbf{B}_{bi} is by means of RPCs which can move along the magnet axis. The length of the coil should be small compared to the cable pitch.

Specific field harmonics can also be determined with longitudinally moving Hall probes or FPCs. The amplitude of the sinusoidally varying field errors is related to \mathbf{B}_{nucd} and \mathbf{B}_{bi} . A configuration of three Hall probes, which could move along the magnet axis, was successfully used to determine small variations of the normal- and skew-sextupole components in the HERA dipole magnets (Brück, '91).

Note that the actual $\mathbf{B}-\dot{B}_{ce}$ curve will deviate from a straight line (see Fig. 7.4) at larger \dot{B}_{ce} i.e. at smaller ramp times because the BICCs, having large characteristic times, cannot attain their steady-state magnitudes during the ramp.

It is possible as well, to distinguish the different field components by analysis of the decay of the field variations in time, as will be shown in section 7.7.1.

7.7 Experimental results of field \mathbf{B}_{cc} in LHC dipole magnets

In the following sections it will be shown that the ISCCs and the BICCs cause considerable field distortions in dipole magnets. In sections 7.7.1-7.7.4 experimental results are presented of fields \mathbf{B}_{is} and \mathbf{B}_{bi} in four LHC dipole model magnets. Field \mathbf{B}_{if} is disregarded since the R_c -values of the magnets are between 1 and 6 $\mu\Omega$ so that $\mathbf{B}_{if} \ll \mathbf{B}_{is}$ (see Table 7.1). The results are obtained on only a few magnets and are used to obtain a first quantitative estimate of the ramp-rate-induced field errors.

The presentation is difficult to survey because the field in the aperture of the magnets is measured by different methods and often under different conditions (see Table 7.5). Furthermore, the measurements are performed using sets of existing non-ideal pick-up coils, with lengths varying between 30 mm and 2000 mm.

Table 7.5. Survey of the type of field measurements which were performed to estimate the field errors \mathbf{B}_{is} and \mathbf{B}_{bi} in four LHC dipole model magnets. #Pos denotes the number of z -positions and #SR denotes the number of field-sweep rates.

Magnet	Length (m)	Hall Probe		FPC			RPC		
		#Pos	#SR	Length (mm)	#Pos	#SR	Length (mm)	#Pos	#SR
CE1	1	1	12	200, 240	5	5	200, 240	5	5
EL2	1	-	-	-	-	-	200	3	3
AN2	10	-	-	750	1	4	30	9 & 5 ^a	1 & 3 ^a
AN3	10	-	-	2000	4 ^b	5	750	4 ^b	4

^a 9 positions at 1 field-sweep rate and 5 positions at 3 sweep rates

^b 2 positions per aperture

Measurements on two 1 m long magnets are performed with pick-up coils at five fixed positions on the axis of the magnet. Two coils, with lengths of 240 mm, cover the ends of the magnet and are referred to as H12 (near the connection end, see Fig. 2.3) and H67 (near the non-connection end). Three coils, with lengths of 200 mm, cover the straight part and are denoted by H3, H4 and H5. The space between the coils is about 4 mm in the axial direction. The lengths of the coils in the straight part correspond to about $1.5L_{p,s}$, so that both \mathbf{B}_{is} and \mathbf{B}_{bi} are measured.

The measurement bench for the 10 m long magnets is provided with a RPC which can be moved in the axial direction. Measurements have been performed with a 750 mm long coil as well as a 30 mm long coil. The axial direction is denoted by z with $z=9.252$ m the axial centre of the magnet. The coils can be moved between $z=3.625$ m (connection end) and $z=12.625$ m (non-connection end). Additionally, measurements are performed with four FPCs of 2000 mm length located in the aperture of the straight part of the 10 m long AN3 magnet.

In the following four sections the results of the field measurements on four magnets, specified in Table 7.5, are discussed. The presence of \mathbf{B}_{is} and \mathbf{B}_{bi} is demonstrated by analysis of the axial variations and the time dependence of \mathbf{B}_{cc} . In section 7.7.5 a survey is given of the main experimental results.

7.7.1 1 m long CE1 magnet

The field component in the y -direction of the CE1 magnet during the second cool-down is determined using a Hall probe located at $x=0$, $y=23$ mm in aperture 1 of the magnet. During and after a field sweep from $B_{ce,2}=3$ T to $B_{ce,1}=0$ T the current as well as the Hall voltage are simultaneously measured for different field-sweep rates \dot{B}_{ce} . In order to express the field during the field sweep, eq. 7.1 is rewritten, assuming that the coupling currents are zero at the beginning of the field sweep:

$$B_y(t) = B_{tr,y} + B_{m,y} + B_{geo,y} + B_{nucd,y} + B_{is,0}(1 - e^{-t/\tau_{is}}) + B_{bi,0}(1 - e^{-t/\tau_{bi}}) \quad [\text{T}], \quad (7.13)$$

with τ_{is} and τ_{bi} the characteristic times of the ISCCs and the BICCs at position $x=0$, $y=23$ mm and t the time (with $t=0$ at the start of the field sweep). The last two contributions can be distinguished by analysing the field after a ramp. A characteristic field variation after a ramp is shown in Fig. 7.5).

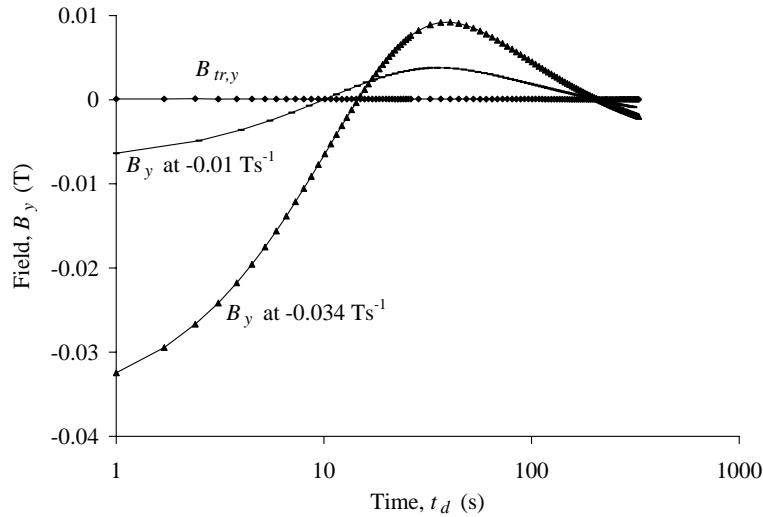


Figure 7.5. The field in the y -direction (see Fig. 2.2a) measured using a Hall probe located at $x=0$, $y=23$ mm in aperture 1 of the CE1 magnet after a ramp from 3 T to 0 T with \dot{B}_{ce} equal to -0.01 Ts^{-1} and -0.034 Ts^{-1} . The time $t_d=0$ corresponds to the end of the ramp. The field produced by the transport current is smaller than 0.1 mT after the field sweep.

Note that the total field still varies, although the cable transport current is 0 (so that also $B_{y,tr}$ is 0 and fields $B_{y,m}$ and $B_{y,geo}$ are constant). Assuming that field $B_{y,nucd}$ remains constant after the ramp, the decay of the field, for all field-sweep rates, can be written as:

$$B_y(t_r, t_d) = C + B_{is,0}(1 - e^{-t_r/\tau_{is}})e^{-t_d/\tau_{is}} + B_{bi,0}(1 - e^{-t_r/\tau_{bi}})e^{-t_d/\tau_{bi}} \quad [\text{T}], \quad (7.14)$$

with C a constant, $t_r=(B_{ce,2}-B_{ce,1})/\dot{B}_{ce}$ the total time of the field sweep and t_d the time after the field sweep. For all sweep rates the time constants τ_{is} and τ_{bi} are deduced to be 10 s and $1.0 \cdot 10^2$ s respectively.

Fields $B_{is,0}$ and $B_{bi,0}$, which are depicted in Fig 7.6, are proportional to \dot{B}_{ce} and have opposite sign. Both the local field $B_{is,0}$ and the local time constant τ_{is} are a factor of about 3 larger than the calculated mean values, assuming a uniform R_c of $1.3 \mu\Omega$ as deduced from the AC-loss measurements (see Table 6.3). The difference implies that locally near the Hall probe R_c is smaller, which can be expected since the last turn of block 6 of this particular magnet is soldered and shunted by a copper strip. The calculated field for $R_c=0.5 \mu\Omega$ is shown in Fig. 7.6 as well.

This result shows that fields \mathbf{B}_{is} and \mathbf{B}_{bi} can be distinguished by analysis of the time dependence of the total field after (but also during) a field sweep. Since the field is only measured at one longitudinal position, the amplitude of \mathbf{B}_{bi} remains unknown.

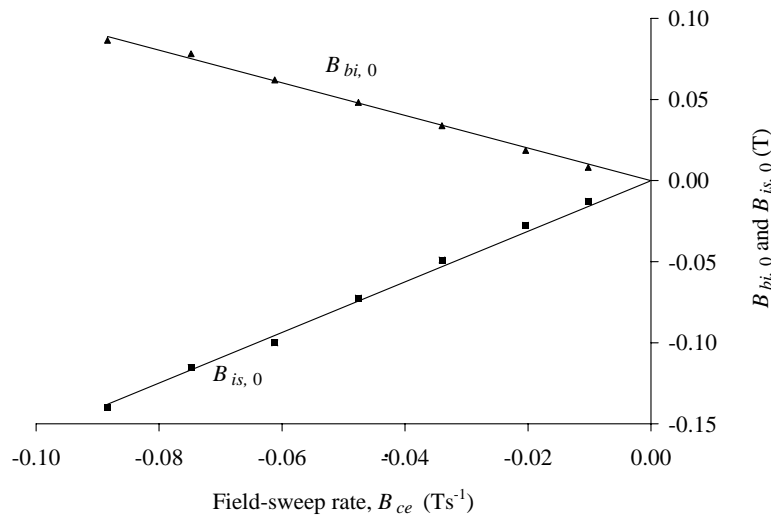


Figure 7.6. The field errors $B_{is,0}$ and $B_{bi,0}$ as functions of the field-sweep rate for the CE1 model, using a Hall probe located at $x=0$, $y=23$ mm. The line through the measured points $B_{bi,0}$ is a best linear fit. The line through the measured points $B_{is,0}$ is the calculated field error for $R_c=0.5 \mu\Omega$.

The FPCs are used to obtain a global value of $B_{cc,y}$ in aperture 1 of the CE1 magnet (during the fourth cool-down). Field B_y is determined with the coils H12, H3, H4, H5 and H67 for field cycles between 2 and 5.4 T at five sweep rates between 0.027 and 0.082 Ts^{-1} . The field error $B_{cc,y}$ at a certain field during the ramp is deduced from the B_y - \dot{B}_{ce} curve (see Fig. 7.4) and depicted in Fig. 7.7.

Field $B_{bi,y}$ is very small compared to field $B_{is,y}$ (so that $B_{cc,y}=B_{is,y}$) because:

- Field $B_{cc,y}$ decays exponentially to 0 after the ramp with a time constant of about 6 s. There is no field contribution present that decays with the expected characteristic time of the BICCs of the order of 10^2 s.
- Field $B_{cc,y}$ is proportional to \dot{B}_{ce} , also for small ramp times of only 40 s. According to Fig. 7.4 this implies that field $B_{cc,y}$ is dominated by the field contribution caused by the ISCCs.

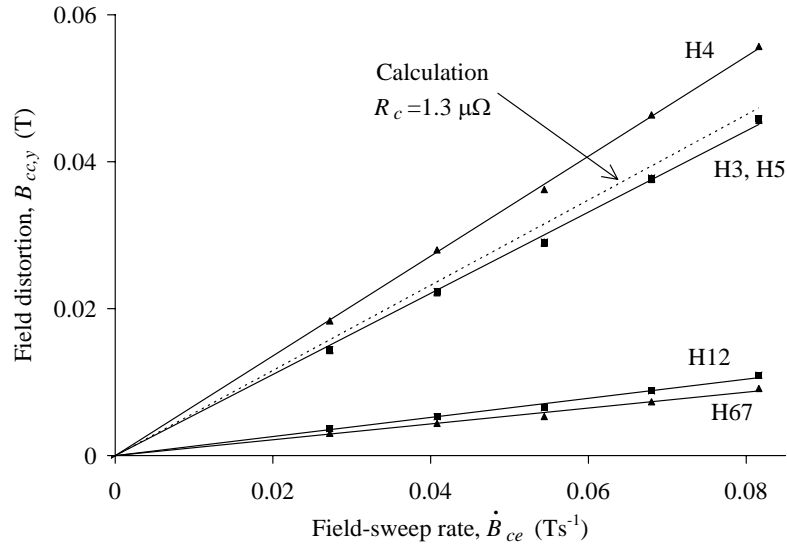


Figure 7.7. The field error $B_{cc,y}$ in aperture 1 of the CE1 magnet as a function of the field-sweep rate, determined by means of FPCs located at five z -positions. The fields deduced using coils H3 and H5 correspond to within 1% of each other. The calculated field distortions for $R_c = 1.3 \mu\Omega$ are shown by a dotted line.

Field $B_{cc,y}$, and hence R_c , are field-independent (between 2 and 5.4 T), which is expected according to the loss measurements (see Table 6.3). Field $B_{cc,y}$ is small in the coil ends because the field component perpendicular to the cable width is small in the ends.

The calculated field distortion $B_{is,y}$ (using Table 7.1 with $R_c = 1.3 \mu\Omega$ as given by Table 6.3) agrees very well with the average field $B_{cc,y}$ in the straight part of the magnet (that is the average of the fields determined using coils H3, H4, H5). An important conclusion is therefore that the field error $B_{is,y}$ can be well calculated from the average R_c and conversely.

The higher harmonics of \mathbf{B}_{cc} are determined by means of RPCs for field cycles between 0.4 and 8.2 T at five field-sweep rates between 0.0068 and 0.034 Ts^{-1} . A characteristic series of measurements is shown in Fig. 7.8 where the skew-quadrupole field a_2 (normalised to the central field) is depicted during the ramp-up and ramp-down for several field-sweep rates. The a_2 component increases with decreasing field since the ISCCs (and hence the skew-quadrupole field A_2) are field-independent. Note that a_2 for $\dot{B}_{ce} = 0.0066 \text{ Ts}^{-1}$ (as anticipated for the operation of LHC) is larger than 10^{-3} at small fields and therefore about one order of magnitude larger than the value that is usually regarded as being acceptable.

The magnitudes of the harmonic components of \mathbf{B}_{cc} are deduced from the $B_n - \dot{B}_{ce}$ and $A_n - \dot{B}_{ce}$ curves, as illustrated in Fig. 7.4. The multipole components for $n=2, 3, 4$ and 5 are shown in Fig. 7.9, scaled to a field-sweep rate of 0.01 Ts^{-1} .

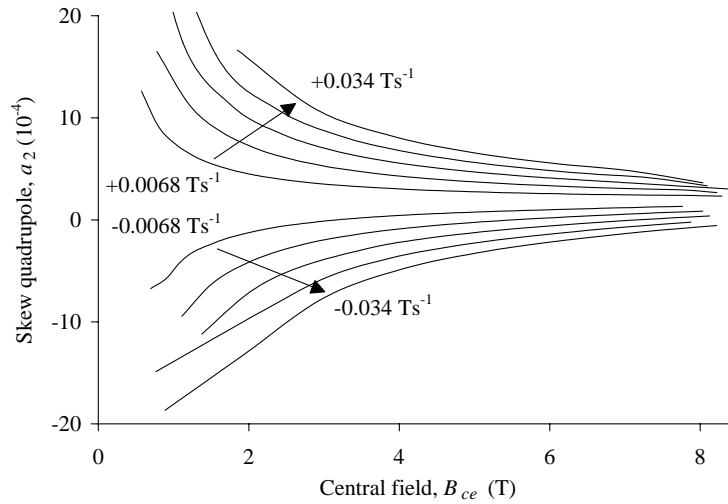


Figure 7.8. The normalised skew-quadrupole component of the CE1 magnet at $x_0=10$ mm, $y_0=0$ during field cycles between 0.4 and 8.2 T with $\dot{B}_{ce}=0.0068, 0.014, 0.020, 0.027$ and 0.034 Ts^{-1} . The field is measured using the RPCs H3 and H4 in series.

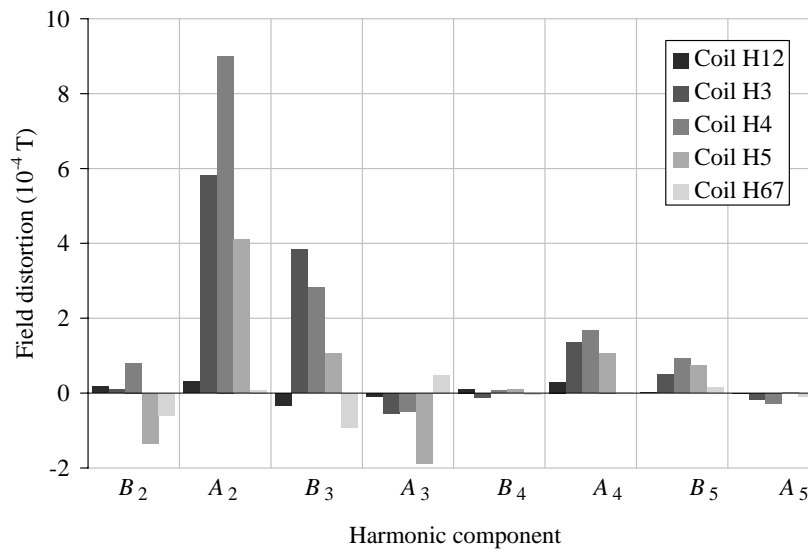


Figure 7.9. The field errors B_{ce} in aperture 1 of the CE1 magnet at $x_0=10$ mm, $y_0=0$ and $\dot{B}_{ce}=0.01$ Ts^{-1} , measured by means of the rotating pick-up coils H12, H3, H4, H5 and H67.

Coils H12 and H67 cover the coil ends where the field normal to the cable width is small. Hence, field B_{is} is small as already observed for the total field (see Fig. 7.7). Coils H3, H4 and H5 cover the straight part of the magnet. Fig. 7.9 shows clearly that most of the multipole components vary considerably over the straight part, which is caused by:

- variations of the R_c -distribution over the cross-section of the coil,
- the contribution from the BICCs, since $l_{coil} \neq kL_{p,s}$, so that a certain part of the sinusoidally varying field \mathbf{B}_{bi} is measured.

Evaluation of the time constants of \mathbf{B}_{cc} after the field sweep (in a similar way as is carried out for the measurements with the Hall probe) shows that most of the variations are due to the BICCs while small differences can be attributed to a varying spatial R_c -distribution along the magnet length. A very rough estimate of fields \mathbf{B}_{is} and \mathbf{B}_{bi} is obtained by assuming that both \mathbf{B}_{is} and the amplitude $\mathbf{B}_{bi,max}$ are constant along the magnet length. Field \mathbf{B}_{cc} for a given \dot{B}_{ce} can then be written as:

$$\mathbf{B}_{cc}(z) = \mathbf{B}_{is} + \mathbf{B}_{bi,max} \sin\left(2\pi(z - z_0) / L_{p,s}\right) \quad [\text{T}]. \quad (7.15)$$

For each component the field contributions caused by the ISCCs and the BICCs as well as the phase $2\pi z_0 / L_{p,s}$ can be deduced by fitting eq. 7.15 to the measured field distortions. The errors in the fields can be large, especially for the higher harmonics, since \mathbf{B}_{is} and $\mathbf{B}_{bi,max}$ are assumed to be z -independent. The results of the fits are given in section 7.7.5.

7.7.2 1 m long EL2 magnet

Only the higher harmonics are measured for this magnet. Field \mathbf{B}_{cc} is determined by means of the RPCs H3, H4 and H5, for field cycles between 2 and 7.5 T at field-sweep rates of 0.0082, 0.016 and 0.033 Ts^{-1} . Coils H12 and H67 are not used to measure the field since the evaluation of the \mathbf{B}_{cc} is too difficult due to the complex geometry of the coil ends.

The multipole components for $n=2, 3, 4$ and 5 of \mathbf{B}_{cc} at $x_0=10$ mm, $y_0=0$ are shown in Fig. 7.10 scaled to $\dot{B}_{ce}=0.01$ Ts^{-1} .

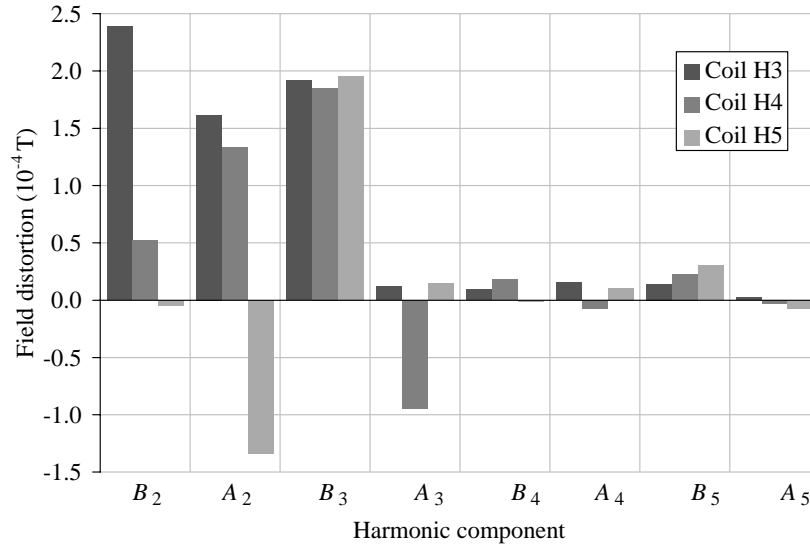


Figure 7.10. The coupling-current induced field B_{cc} of the EL2 magnet at $x_0=10$ mm, $y_0=0$ and $\dot{B}_{ce}=0.01$ Ts^{-1} , measured by means of the rotating pick-up coils H3, H4 and H5.

The field distortions are of the same order as those observed in the CE1 magnet except for the A_2 component which is about one order of magnitude smaller. This implies that the difference $|1/R_{c,P1}-1/R_{c,P2}|$ in the EL2 magnet is smaller than in the CE1 magnet.

Analysis of the time dependence of the harmonics shows that the components B_2 , A_2 and A_3 are dominated by the fields caused by the BICCs while the fast decay of the B_3 component after a ramp implies that this multipole is mainly caused by ISCCs. The almost constant B_3 implies that R_c is almost z -independent. The octupole and decapole components are small compared to the lower harmonics and are not further discussed. Fields \mathbf{B}_{is} and \mathbf{B}_{bi} are estimated by fitting eq. 7.15 to each multipole component, and presented in section 7.7.5.

7.7.3 10 m long AN2 magnet

In the case of the AN2 magnet, field $B_{cc,y}$ is determined using the 750 mm long FPC (so that $l_{coil}=5.8L_{p,s}$) located near the axial centre of the magnet. By using such a long pick-up coil the measured field $B_{cc,y}$ is likely to be dominated by $B_{is,y}$, since the enclosed flux caused by the BICCs is relatively small. Field $B_{cc,y}$ is measured during four field cycles between 0 and 4.1 T at four different field-sweep rates and shown in Fig. 7.11.

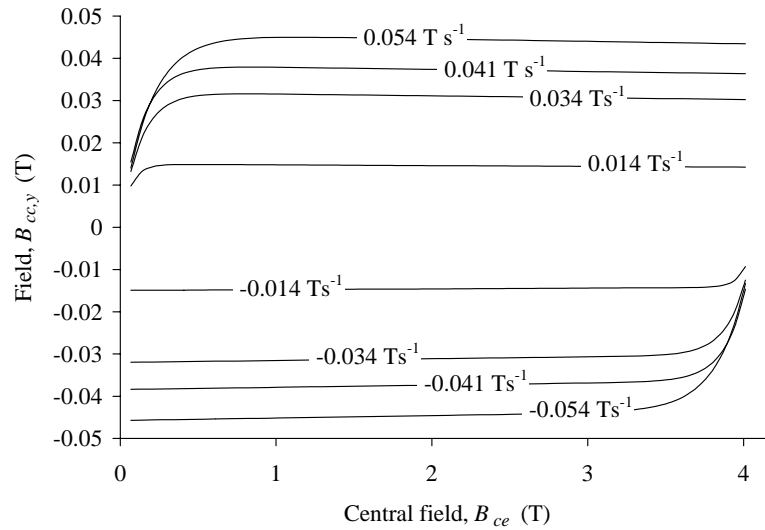


Figure 7.11. The field error $B_{cc,y}$ in aperture 1 of the AN2 magnet as a function of the central field during field cycles between 0 and 4.1 T at four field-sweep rates.

Field $B_{cc,y}$ is field-independent and exhibits a time constant of about 4 s, which is about twice as large as the time constant $\tau_{is,M}$ deduced from the loss measurements during ramping (see Table 6.3). The absence of large characteristic times shows that $B_{cc,y}$ is mainly caused by the ISCCs, as expected from the large coil length. The field error is about 10% more than the value calculated using Table 7.1 with an average R_c of 1.3 $\mu\Omega$ in aperture 1 (see Fig. 6.6 and the text below this figure).

An important conclusion is therefore that a measurement by means of a long FPC of field $B_{cc,y}$ as a function of \dot{B}_{ce} results in a good estimate of R_c . At the same time it is possible to investigate the field dependence of R_c .

In the rest of this section field \mathbf{B}_{bi} is investigated by means of the 30 mm long RPC. The decay of the higher field harmonics is measured at nine z -positions after a field sweep from 7.5 T to 0.4 T at -0.034 Ts^{-1} . As an example the decay of the B_3 component is depicted in Fig. 7.12.

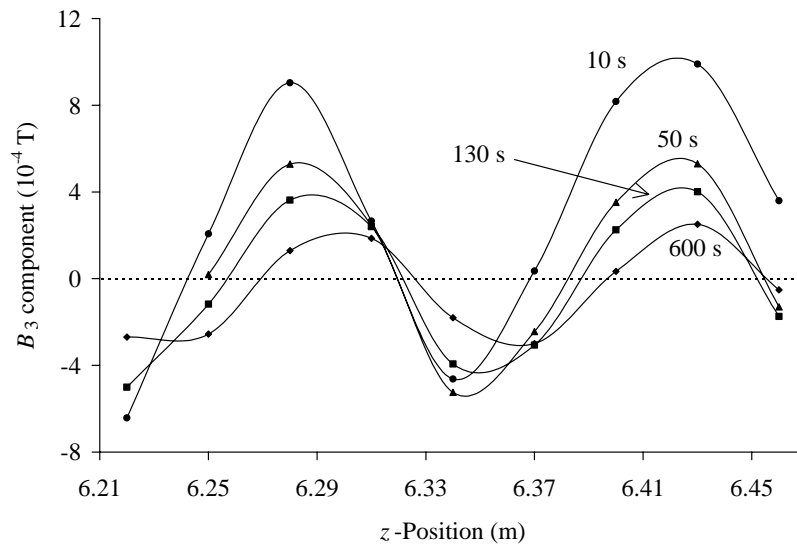


Figure 7.12. Decay of the B_3 component in aperture 1 of the AN2 magnet at $x_0=10 \text{ mm}$, $y_0=0$ after a ramp down from 7.5 T to 0.4 T at $\dot{B}_{ce}=-0.034 \text{ Ts}^{-1}$. The field is measured by means of the 30 mm long RPC at nine z -positions spaced 30 mm apart.

During the decay the *average* B_3 -value decreases from about $2 \cdot 10^{-4} \text{ T}$ to 0 in the first seconds due to the decay of the ISCCs. What is left after a few seconds is a sinusoidally varying field which can be regarded as a superposition of fields B_{bi} and B_{nucd} . The former decays with a characteristic time τ_{bi} of about 10^2 s . The latter remains constant in time until the measurement ends after 600-1000 s. An important conclusion is that τ_{bi} is about the same as the τ_{bi} of the 1 m long CE1 and EL2 magnets. Therefore, the characteristic time τ_{bi} seems to be independent of the length of the magnet.

Note, that not only the amplitude but also the phase of the sinusoidal pattern changes during the decay since B_{bi} and B_{nucd} have a different phase. Most of the multipoles show a similar decay with characteristic times:

- of several seconds related to the decay of the ISCCs,
- of about 10^2 s related to the decay of the BICCs,
- much larger than 10^3 s attributed to a NUCD.

In order to investigate whether the remaining field pattern is really independent of \dot{B}_{ce} , as expected from Table 7.4 in the case of a NUCD, field B_{cc} is determined at three different field-sweep rates ($\dot{B}_{ce}=0.014, 0.024$ and 0.034 Ts^{-1}). The central field is cycled between 0.6 and 7.5 T and the field is measured at five z -positions. Fig. 7.13 depicts the characteristic decay of the normal quadrupole after a ramp up with $\dot{B}_{ce}=0.014$ and 0.034 Ts^{-1} .

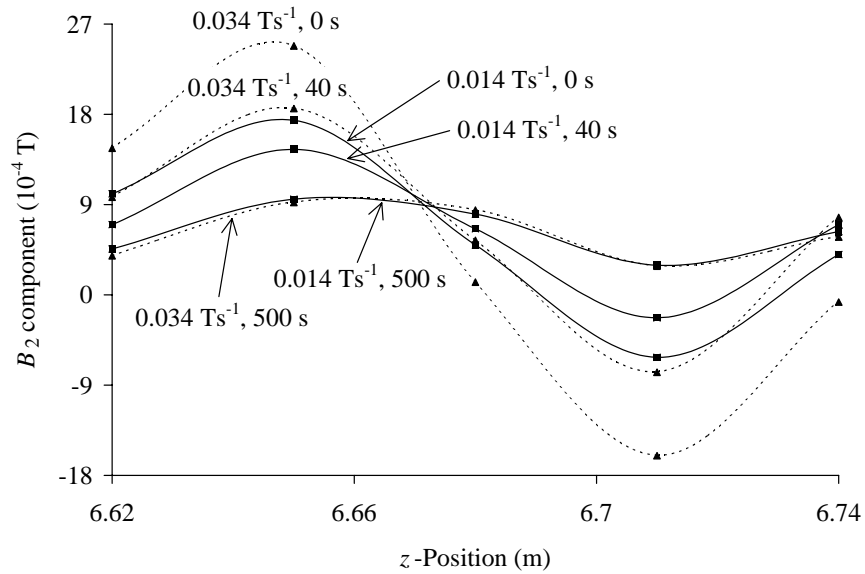


Figure 7.13. Decay of the B_2 component in aperture 1 of the AN2 magnet at $x_0=10 \text{ mm}$, $y_0=0$ after a ramp up from 0.6 T to 7.5 T. The field is measured using the 30 mm long RPC at five z -positions. The labels indicate the field-sweep rate and the time after the end of the ramp.

The field caused by the ISCCs is very small, since the average B_2 -value remains constant during the decay. The amplitude of the B_2 component, caused by the BICCs, increases with increasing field-sweep rate and decays with a characteristic time τ_{bi} of about 10^2 s . After a time $t_d \gg \tau_{bi}$ the field pattern becomes constant and *independent of the field-sweep rate* of the preceding ramp. The remaining field pattern is therefore caused by a non-uniform current distribution among the strands exhibiting very large characteristic times.

The harmonic coefficients of \mathbf{B}_{cc} are determined from the slope of the $\mathbf{B}-\dot{B}_{ce}$ curve in the same way as for the CE1 and EL2 magnets. The results, scaled to $\dot{B}_{ce}=0.01 \text{ Ts}^{-1}$, at five z -positions are shown in Fig. 7.14.

Note the very strong variations of especially the B_2 , A_2 and B_3 components caused by the BICCs. The magnitudes of the multipole coefficients of \mathbf{B}_{is} and \mathbf{B}_{bi} individually, are estimated by fitting eq. 7.15 to the values of each component of \mathbf{B}_{cc} at the five z -positions. The results of the fits and the conclusions are presented in section 7.7.5.

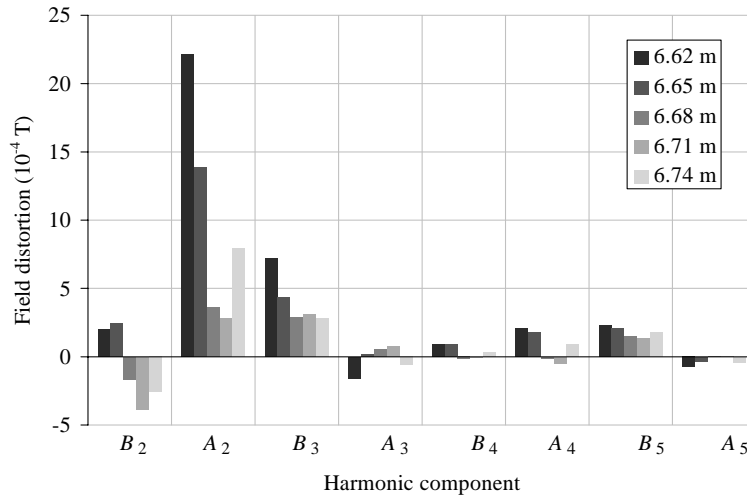


Figure 7.14. The field \mathbf{B}_{cc} in aperture 1 of the AN2 magnet at $x_0=10$ mm, $y_0=0$ and $\dot{B}_{ce}=0.01$ Ts⁻¹, measured by means of the 30 mm long RPC, located at five z -positions spaced 30 mm apart.

7.7.4 10 m long AN3 magnet

The coupling-current induced field \mathbf{B}_{cc} of the AN3 magnet is evaluated from the field determined by the 750 mm long RPC using cycles between 0.6 and 8.2 T at $\dot{B}_{ce}=0.0068$, 0.014, 0.024 and 0.034 Ts⁻¹. Note that the enclosed flux due to the BICCs is probably small compared to that caused by the ISCCs since the coil length is 6.25 times the cable pitch. The field determined in both apertures at two different z -positions is shown in Fig. 7.15.

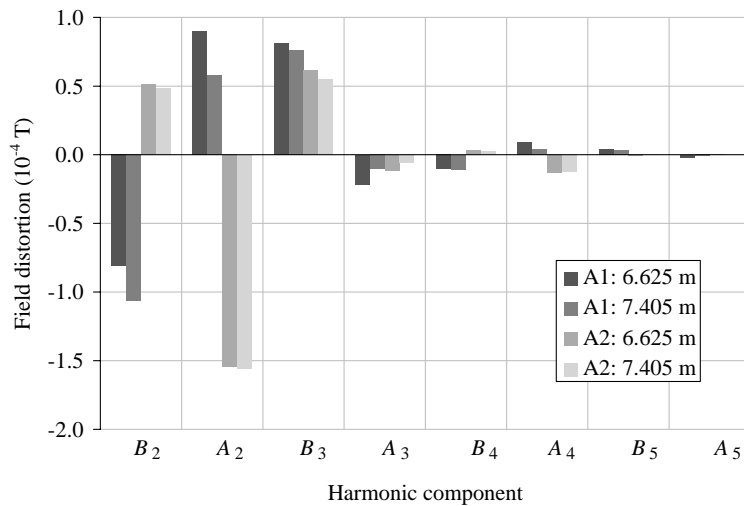


Figure 7.15. The field B_{cc} of the AN3 magnet at $x_0=10$ mm, $y_0=0$ and $\dot{B}_{ce}=0.01$ Ts⁻¹ determined by means of the 750 mm long RPC located at two z -positions in the apertures A1 and A2.

The signs of the fields are relative to the sign of the main field in that aperture. This implies that, according to Table 7.1, the B_3 and B_5 components are positive. Note that the much smaller B_3 component compared to the AN2 magnet, is inherent to the much larger R_c of the AN3 magnet (see Table 6.4).

The opposite sign of the A_2 and A_4 multipoles in both apertures indicates that the R_c -values in the poles A11 and A21 are larger than in the poles A12 and A22 respectively (see Fig. 6.4b).

The difference in the magnitude of the A_2 and A_4 components in the two apertures shows that the difference between R_c in the two poles of aperture 1 is smaller than that in the two poles of aperture 2.

7.7.5 Evaluation of fields \mathbf{B}_{is} and \mathbf{B}_{bi}

In Table 7.6 a survey is given of the coupling current induced field errors \mathbf{B}_{is} and \mathbf{B}_{bi} which are determined by fitting eq. 7.15 to the measured field errors \mathbf{B}_{cc} . The fit is only made for the CE1, EL2 and AN2 magnets.

Table 7.6. Survey of the harmonic distortions \mathbf{B}_{is} and \mathbf{B}_{bi} (in 10^{-4} T) at $x_0=10$ mm, $y_0=0$ in four LHC dipole model magnets at $\dot{B}_{ce}=0.01$ Ts $^{-1}$. The B_y -value is determined by means of the FPCs while the higher harmonics B_2 - A_5 are determined by means of the RPCs.

	1 m long CE1, Aperture 1			1 m long EL2		
	$B_{is,exp}$	$B_{bi,exp}$	$B_{is,calc}$	$B_{is,exp}$	$B_{bi,exp}$	$B_{is,calc}$
$R_{c,P1}$	1.6 $\mu\Omega$			2.8 $\mu\Omega$		
$R_{c,P2}$	2.0 $\mu\Omega$			3.0 $\mu\Omega$		
B_y	+64	-	+67	-	-	+30
B_2	+0.047	8.5	-	+0.87	13	-
A_2	+6.9	14	+2.6	+0.70	16	+0.61
B_3	+2.6	15	+1.52	+1.9	0.31	+0.94
A_3	-0.88	7.3	-	-0.37	2.8	-
B_4	+0.032	1.1	-	+0.10	0.69	-
A_4	+1.4	1.9	-0.29	+0.033	0.60	+0.068
B_5	+0.76	1.6	-0.15	+0.22	0.84	-0.094
A_5	-0.18	1.1	-	-0.028	0.51	-

	10 m long AN2, Aperture 1			10 m long AN3, Aperture 1		10 m long AN3, Aperture 2	
	$B_{is,exp}$	$B_{bi,exp}$	$B_{is,calc}$	$B_{cc,exp}$	$B_{is,calc}$	$B_{cc,exp}$	$B_{is,calc}$
$R_{c,P1}$	1.2 $\mu\Omega$			6.2 $\mu\Omega$		6.8 $\mu\Omega$	
$R_{c,P2}$	1.4 $\mu\Omega$			6.0 $\mu\Omega$		5.7 $\mu\Omega$	
B_y	+75	-	+68	-	+13	+9.1	+13
B_2	-0.17	3.5	-	-0.94	-	+0.50	-
A_2	+12	9.9	+3.8	+0.74	+0.12	-1.6	-0.61
B_3	+4.5	2.4	+2.1	+0.79	+0.41	+0.58	+0.41
A_3	-0.30	1.0	-	-0.16	-	-0.088	-
B_4	+0.49	0.58	-	-0.11	-	+0.030	-
A_4	+1.0	1.2	+0.42	-0.067	+0.013	-0.13	-0.068
B_5	+1.9	0.46	-0.21	+0.037	-0.041	-0.0026	-0.041
A_5	-0.35	0.37	-	-0.016	-	+0.00051	-

The error in the presented values is about 10% for B_y , and about 20-40% for the higher harmonics. In the case of the AN3 magnet, field \mathbf{B}_{is} is deduced from the average field \mathbf{B}_{cc} measured by means of the 750 mm long RPC at the two z -positions. Field \mathbf{B}_{bi} is disregarded since the total length of 1.5 m is about $11.5L_{p,s}$.

The normal-odd harmonics of \mathbf{B}_{is} are calculated using Table 7.1 with an average R_c based on the results of the loss measurements. The skew-even harmonics of \mathbf{B}_{is} are calculated using Table 7.3 with contact resistances $R_{c,p1}$ and $R_{c,p2}$ in the two poles of an aperture estimated from the loss measurements on the separate poles.

Table 7.6 shows that the calculated and experimentally determined values of $B_{is,y}$ correspond well, while for the B_3 component differences of about a factor 2 are observed. In order to meet the field accuracy, it is therefore preferable to have an R_c -value of the cable which is about a factor 2 larger than the calculated minimum value (see section 7.4).

Large A_2 components are observed for the magnets with large differences between R_c of the two poles of the same aperture. Because the resistances $R_{c,p1}$ and $R_{c,p2}$ are estimated values, the skew-even harmonics cannot be calculated exactly. However, the measurements on the AN3 show that for $R_c > 10 \mu\Omega$ (as stated in section 7.4) the A_2 and A_4 multipole components will probably be smaller than 10^{-4} T.

In the case of the higher multipoles the discrepancy between the measurements and the calculations becomes larger due to the stronger sensitivity of the multipoles to local R_c variations.

No direct correlation is present between R_c and the estimated field \mathbf{B}_{bi} . Especially the amplitude of the quadrupole and sextupole components (both the skew and the normal) are well above 10^{-4} T at $x_0 = 10$ mm, $y_0 = 0$.

The results of these incidental measurements on the four magnets show that the time constant of about 10^2 s seems to be independent of R_c and the length of the magnet. This implies, according to eqs. 5.13 and 5.14, that the BICCs should be classified in regime A, and hence flow over an average characteristic length which is much smaller than the length of the cable. The effective strand resistivity and the characteristic length can be roughly estimated by using the formulas for a straight cable (eqs. 5.13 and 5.8):

$$\rho_s = 2 \cdot 10^{-8} \frac{N_s \pi d_s^2}{\tau_{bi}} = 2.8 \cdot 10^{-14} \quad [\Omega\text{m}], \quad (7.16)$$

and:

$$\xi = 0.50 \sqrt{\frac{R_c L_{p,s} \pi d_s^2}{2 \rho_s N_s}} = 3.5 \cdot 10^2 \sqrt{R_c} \quad [\text{m}]. \quad (7.17)$$

Since the various turns probably cause a reduction of the average time constant compared to a straight cable, ρ_s can decrease to about 10^{-14} Ωm and ξ can increase by about a factor 2. This leads to a characteristic length of about 0.5 to 2 m for $1 < R_c < 7 \mu\Omega$.

The origin of the large effective strand resistivity that the BICCs ‘see’ is not well-known. It is certain that it cannot be attributed to the dynamic resistivity, which is linear to the field change $\dot{B}_{\perp s}$ (see eq. 3.6), since τ_{bi} and hence ρ_s are independent of the field-sweep rate.

According to the treatment of BICCs in chapter 5, BICCs can only decay exponentially along the cable length if a certain voltage is present over the strand sections between two nodes of the network model. In the network model, this implies that the strand sections have to be resistive since the voltages over the resistances R_c are assumed to have no x - or z -components. However, a current through R_c has to flow from the filaments of one strand to the filaments of the other strand and in this process will pass through the copper outer shell of the strands (see Fig. 2.9a) and through part of the matrix. This transfer causes not only a voltage in the y -direction but locally also a voltage in the axial direction (as well as in the x -direction). It has to be investigated in detail whether the large effective strand resistivity can be attributed to the small axial resistive voltage caused by the currents through R_c .

7.8 Conclusions

In a magnet made of a multistrand superconductor three field components are present which depend linearly on the central-field-sweep rate \dot{B}_{ce} , namely:

- the field \mathbf{B}_{if} produced by the IFCCs,
- the field \mathbf{B}_{is} produced by the ISCCs,
- the field \mathbf{B}_{bi} produced by the BICCs.

Field \mathbf{B}_{if} can be calculated by representing the screening-current density in the strands by two currents of opposite sign located at the centre of gravity of half a strand. The field \mathbf{B}_{if} in the aperture of an LHC dipole is smaller than $0.1 \cdot 10^{-4}$ T at $x_0=10$ mm, $y_0=0$ for all multipole components (assuming the characteristic values $\tau_{if}=0.025$ s and $\dot{B}_{ce}=0.01$ Ts⁻¹), and is negligible compared to the field produced by the filament magnetisation and the field distortions caused by fabrication tolerances.

Field \mathbf{B}_{is} is calculated by representing all the zigzag ISCCs as infinitely long straight line currents. Field \mathbf{B}_{is} is inversely proportional to the cross-contact resistance R_c and increases strongly for increasing cable width. Since the ISCCs follow the symmetry of the field generated by the transport current, only the normal-odd harmonics are affected if the R_c -distribution is uniform over the cross-section of the magnet. Calculations and measurements of various LHC dipole magnets are in good agreement and show that mainly the B_1 and B_3 components are large. Characteristic values are about $24 \cdot 10^{-4}$ T and $0.7 \cdot 10^{-4}$ T respectively (at $x_0=10$ mm, $y_0=0$) for $R_c=3 \mu\Omega$ and $\dot{B}_{ce}=0.01$ Ts⁻¹. The measurements have shown that R_c varies by less than 10-20% along the length of the straight part of a coil and that R_c is independent of the current and field levels.

In the case of non-uniform R_c -distributions the other field harmonics are also affected. Especially the skew-quadrupole component can be large due to a difference in R_c between the two poles of an aperture. In the LHC dipole model magnets A_2 -values of up to $10 \cdot 10^{-4}$ T (at $x_0=10$ mm, $y_0=0$) at $\dot{B}_{ce}=0.01$ Ts⁻¹ are observed. The measured fields are in fair

agreement with calculated values based on the average R_c -values as deduced from the loss measurements. While the B_1 and B_3 components have the same direction in all the coils, the sign of the skew-even harmonics is probably non-systematic.

Reduction of \mathbf{B}_{is} is possible by a decrease of the field-sweep rate and by an increase of R_c . An R_c -value of $10 \mu\Omega$ would limit the field errors in LHC dipole magnets to acceptable values while the total ramp time from injection field to operation field remains below 30 minutes.

An important conclusion is that the contact resistance between the strands of a cable has to be increased for dipole magnets (with a ‘two-shell’ geometry) having a larger central field in order to meet a field homogeneity of the order of 10^{-4} .

Field \mathbf{B}_{bi} can be determined by calculating the BICCs taking into account the exact spatial field distribution in the coil. The pattern of \mathbf{B}_{bi} along the magnet axis is always (quasi-)sinusoidal with an amplitude proportional to \dot{B}_{ce} and a period equal to the transposition length. The amplitude of \mathbf{B}_{bi} is difficult to calculate since the magnitude of the BICCs depends strongly on the exact geometry of the magnet and on spatial variations of the contact resistance and the strand resistivity. Simulations show that especially the quadrupole and sextupole components (both normal and skew) can attain large values. Experimental results on LHC dipole magnets show that the amplitude of these multipoles can be as large as $20 \cdot 10^{-4}$ T (at $x_0=10$ mm, $y_0=0$ and $\dot{B}_{ce}=0.01$ Ts $^{-1}$). In the absence of sufficient measurements it is not sure what causes the differences in \mathbf{B}_{bi} between the four magnets that are measured.

The BICCs of the 1 m as well as the 10 m long LHC dipole model magnets exhibit characteristic times of about 10^2 s. These times seem to be not only independent of the magnet length but also of R_c . This implies that the BICCs decay with a characteristic length ξ which is much smaller than the length of the cable. For the four investigated magnets the characteristic length is estimated to be about 0.5-2 m. Calculations demonstrate that, in this case, the BICCs cause a voltage over the strands which would correspond to an effective strand resistivity ρ_s of about 10^{-14} Ω m. This resistivity can be related to the diffusion process of the coupling currents from the contacts into the filaments, but a more detailed investigation of this process is required in order to support this explanation.

In coils made of multistrand conductors a third additional field \mathbf{B}_{mucd} is present, besides fields \mathbf{B}_{is} and \mathbf{B}_{bi} , caused by a non-uniform distribution of the transport current among the strands. This field varies sinusoidally along the magnet length with a period equal to the cable pitch and exhibits a characteristic time which is much larger than 10^3 s. The value of the field is independent of the field-sweep rate of the preceding ramp.

Sinusoidal variations of the field along the magnet axis as observed in superconducting magnets are a superposition of fields \mathbf{B}_{bi} and \mathbf{B}_{mucd} . Which of these fields is dominant depends mainly on the excitation level, the field-sweep rate, the spatial R_c - and ρ_s -distributions and the uniformity of the soldered cable-to-cable connections. In general, field \mathbf{B}_{bi} becomes relatively more important when the size of the cable increases and the contact resistances between strands decrease.